JACS
JOURNAL OF THE AMERICAN CHEMICAL SOCIETY
pubs.acs.org/JACS
Article

Confinement of 1D Chain and 2D Layered CuI Modules in K-INA-R Frameworks via Coordination Assembly: Structure Regulation and Semiconductivity Tuning

Zhao-Feng Wu,[∇ Z.-F.W. and C.W.] Chuanzhe Wang,[∇ Z.-F.W. and C.W.] Xingwu Liu,* Kui Tan, Zhihua Fu, Simon J. Teat, Zi-Wei Li, Xiuze Hei, Xiao-Ying Huang, Gang Xu,* and Jing Li*

Cite This: *J. Am. Chem. Soc.* 2023, 145, 19293−19302

Read Online

ACCESS | Metrics & More | Article Recommendations | Supporting Information

ABSTRACT: Herein, we present a new series of CuI-based hybrid materials with tunable structures and semiconducting properties. The CuI inorganic modules can be tailored into a one-dimensional (1D) chain and two-dimensional (2D) layer and confined/stabilized in coordination frameworks of potassium isonicotinic acid (HINA) and its derivatives (HINA-R, R = OH, NO_2, and COOH). The resulting CuI-based hybrid materials exhibit interesting semiconducting behaviors associated with the dimensionality of the inorganic module; for instance, the structures containing the 2D-CuI module demonstrate significantly enhanced photoconductivity with a maximum increase of five orders of magnitude compared to that of the structures containing the 1D-CuI module. They also represent the first CuI-bearing hybrid chemiresistive gas sensors for NO_2 with boosted sensing performance and sensitivity at multiple orders of magnitude over that of the pristine CuI. Particularly, the sensing ability of CuI-K-INA containing both 1D- and 2D-CuI modules is comparable to those of the best NO_2 chemiresistors reported thus far.

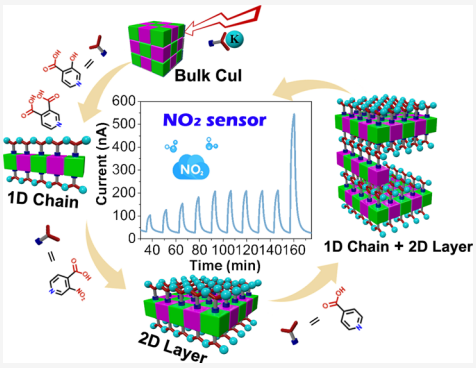

■ INTRODUCTION

As an important family of Cu(I)-based semiconductors, binary copper halides (CuX, X = Cl, Br, I) have been extensively investigated for their applications in photodetectors, piezoelectrics, and transparent transistors to name a few.[1] In recent years, some pioneering research has been reported on the exploration of bulk CuX as chemiresistive gas sensors. For instance, CuBr has been used in sensing of NH_3,[2] while CuI was tested for detecting greenhouse gases.[3] However, such examples are quite limited and some challenges are yet to be overcome. Taking CuI for example, the high operational temperature, relatively low response, and selectivity compared to conventional inorganic sensors have impeded its utility as popular chemiresistors.[3] Therefore, developing new strategies to tailor bulk CuX semiconductors to improve their chemiresistive gas sensing performance is of vital importance.

The rapid development of coordination polymers (CPs) in the past two decades has led to the discovery of numerous hybrid structures where functional inorganic network modules are confined in the ordered CP backbone, endowing them with novel properties that are distinct from the pristine inorganic phases.[4] CuI module-bearing CPs are the most reported examples for CuX hybrids. Compared with the previously reported CuI(L) hybrid materials where CuI modules only coordinate to organic ligands (L),[5] the formation of hybrid structures where these inorganic modules are assembled within CP networks via various coordination modes between the metal and organic building units would result in much more abundant structure types. The confinement of extended inorganic CuI modules in CPs would offer a new strategy in tuning and optimizing chemiresistive sensing properties, such as increasing sensing selectivity and sensitivity and lower operating temperature. Compared with the pristine CuI with a wide band gap,[1f,6] the optical absorption of the resulting hybrid compounds will be extended to longer wavelength (lower-band-gap) region through energy transfer between inorganic and organic modules, and the sensing parameters may be further optimized under lower-energy light irradiation. Thus far, CPs containing ordered higher-dimensional CuI arrays such as 1D chain and especially 2D layer are very rare and all of them are made of rare earth elements (REEs) with little known about their physical properties.[7] To the best of our knowledge, REE-free CPs containing 1D- or 2D-CuI inorganic motifs have never been reported to this date.

Herein, we report a series of K-INA-R CPs (R = H, OH, NO_2, and COOH) incorporating 1D- and 2D-CuI inorganic

Received: May 16, 2023
Published: August 24, 2023

https://doi.org/10.1021/jacs.3c05095
J. Am. Chem. Soc. 2023, 145, 19293−19302

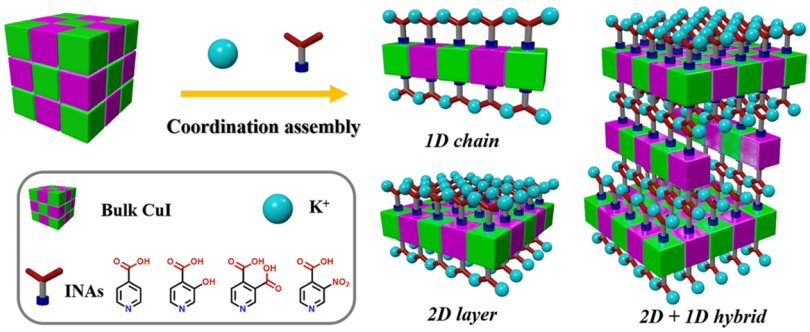

Figure 1. Schematic illustration of the confinement of 1D chain and/or 2D layered CuI modules assembled in K-INA-R CPs.

modules with the formula [K_2CuI(INA-COO)DMF] (CuI-K-INA-COOH, INA-COOH = 3,4-pyridinedicarboxylic acid), [$K_{10}Cu_9I_9$(INA-OH)$_{10}$] (CuI-K-INA-OH, INA-OH = 3-hydroxy-4-pyridinecarboxylic acid), KCuI(INA-NO_2) (CuI-K-INA-NO_2, INA-NO_2 = 3-nitro-4-pyridinecarboxylic acid), and [$K_{10}Cu_9I_7$(INA)$_{12}$(H_2O)] (CuI-K-INA, INA = isonicotinic acid), as well as a detailed study of their semiconducting properties. The bulk CuI could be tailored into 1D- and 2D-CuI modules by coordination assembly and periodically confined in K-INA-R frameworks (Figure 1). The semiconducting properties of the resulting hybrid structures depend largely on the dimensionality of the CuI modules. For instance, the photoconductivity is increased by orders of magnitude going from CuI-K-INA-COOH and CuI-K-INA-OH (with CuI 1D chain) to CuI-K-INA-NO_2 (containing CuI 2D layer). In particular, both 1D chain and 2D layered CuI inorganic modules can be integrated into one structure as in the case of CuI-K-INA and compared with the pristine CuI sensor that only works under elevated temperature with low selectivity and sensitivity; the chemiresistive sensing performance of CuI-K-INA for NO_2 is increased by multiple orders of magnitude at room temperature (RT). This work represents the first gas sensing study of CuX-bearing CPs, which demonstrate performances comparable to the best chemiresistors based on metal oxides, metal dichalcogenides, nanocarbons, and others. This work offers a new approach to designing novel chemiresistive sensing materials by tailoring conventional semiconductors in conductive hybrids via coordination assembly.

■ RESULTS AND DISCUSSION

Structure Analysis. The title compounds were obtained by solvothermal reactions of CuI, KI, INA, and its derivatives (INA-R, R = OH, NO_2, and COOH) in mixed solvents of DMF, CH_3CN, and ethanol (Figures S1−S4). The crystal structures were analyzed by the single-crystal X-ray diffraction (SCXRD) method. By varying the functional group (R) of −OH, −COOH, and −NO_2 in the meta-position of the pyridine ring of INA, different 1D and 2D inorganic CuI modules can be incorporated into the K-INA-R networks (Figure 1). In CuI-K-INA-COOH, each K(1)$^+$ ion is seven-coordinated by two oxygen atoms from two DMF and five oxygen atoms from four carboxylate groups of INA-COO$^-$, while each K(2)$^+$ ion is six-coordinated by six carboxylate groups from INA-COO$^-$. The K$^+$ cations are interconnected by sharing the COO$^-$ groups to generate a 2D K−O layer, and the pyridines in INA-COO$^-$ suspended on the K−O layer coordinate to 1D-(CuI)$_n$ chains via N-Cu dative bonds (Figures S5 and S6).[7c,d] In CuI-K-INA-OH, due to the different coordinate modes of the carboxyl and −OH groups, the K atoms are seven-coordinated by four different carboxyl groups to form 1D K−O double chain, and the −OH groups of INA-OH further bridge the neighboring K−O double chains to generate 2D K-carboxyl and −OH coordination layers. The pyridines in INA-OH are suspended on both sides of the layers (Figures S7 and S8). To cope with the configuration of K−O chains, the distorted 1D staircase-like (CuI)$_n$ chains were formed and confined in the 3D structure of CuI-K-INA-OH (Figure S8).[8] As for CuI-K-INA-NO_2, each K$^+$ cation is nine-coordinated by oxygen atoms from four carboxyl groups and one nitro group, and the nitro and carboxyl groups in INA-NO_2 adopt a chelating coordination mode bonding to K$^+$ cations to form a 2D K−O layer, while the INA-NO_2 ligands are stacked in a staggered mode (Figures 2a and S9). The two neighboring pyridines hanging on the K−O planes adopt a head-to-head configuration and bridge two CuI modules to form a {Cu_2I_2} rhombohedron. Each {Cu_2I_2} is further bridged to the four adjacent {Cu_2I_2} dimers through the Cu−I−Cu linkage to form a 2D inorganic (CuI)$_n$ layer (Figure 2a, highlighted in a dotted line) and confined in the 3D CuI-K-INA-NO_2 (Figures S9f and S10). Use of the pristine INA ligand yields CuI-K-INA where K$^+$ ions are linked through the carboxyl groups to form a K-COO layer (Figure 2b). However, the stacking arrangements of the INA ligands above and below the K−O layer adopt a variety of coordination modes (named L1−L6 for clarity), very different from the other three compounds (Figure S11). On one side of the K-carboxyl layer, L1 and L3 are parallel but not overlapping and stack in a similar fashion as those in CuI-K-INA-COOH to CuI-K-INA-NO_2, resulting in the same 1D-CuI chains as in CuI-K-INA-COOH (Figure S6c). However, the neighboring terminal DMF molecules in CuI-K-INA-COOH are replaced by INA (type L2) in CuI-K-INA, and L2 with a pyridine ring perpendicular to L1 and L3 adopts a head-to-head fashion to bridge Cu atoms with the neighboring L2 and further connects the 1D-CuI chains through the Cu−I coordination (Cu−I bond value is 2.81 Å) to form a 2D-CuI layer viewed along the *bc* plane in CuI-K-INA (Figure 2b, highlighted in blue line). On the other hand, the L4, L5, and L6 show a face-to-face manner and overlap each other to bridge the CuI to form 1D-CuI chains that are similar to the CuI chain module in CuI-K-INA-NO_2 (Figures S9f and S11c).[9] This is an unprecedented example of confined CuI modules with both 1D chains and 2D layers of CuI within one structure (Figure S12). Compared with the previously reported CuI hybrid compounds assembled with only organic ligands,[5] the coordination of a CP network and various CuI modules in a crystal lattice offers many more possible coordination modes between the two counterparts

https://doi.org/10.1021/jacs.3c05095
J. Am. Chem. Soc. 2023, 145, 19293−19302

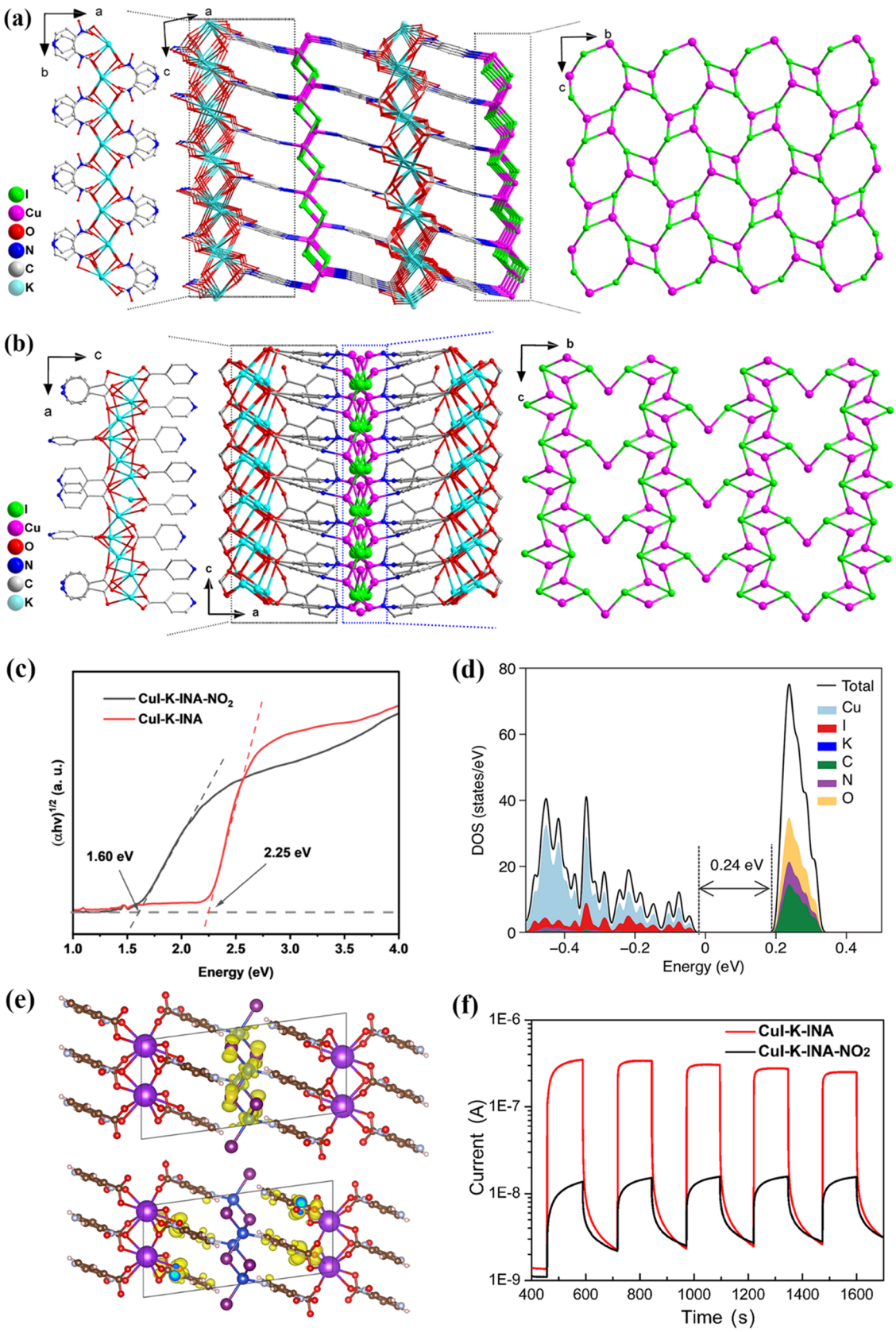

Figure 2. Coordination of metals and crystal structures of (a) CuI-K-INA-NO_2 and (b) CuI-K-INA with K-INA-R and 2D-CuI modules highlighted in dotted lines. (c) The Tauc plots of CuI-K-INA-NO_2 and CuI-K-INA. Insets are the photographs of the as-made crystal samples. (d) The density of states (DOS) plots of CuI-K-INA-NO_2. (e) The plot of the highest occupied crystal orbital of VB (top) and lowest unoccupied crystal orbital of CB (bottom) of CuI-K-INA-NO_2. (f) The light responding conductivity plots for CuI-K-INA-NO_2 and CuI-K-INA under visible light.

https://doi.org/10.1021/jacs.3c05095
J. Am. Chem. Soc. 2023, 145, 19293−19302

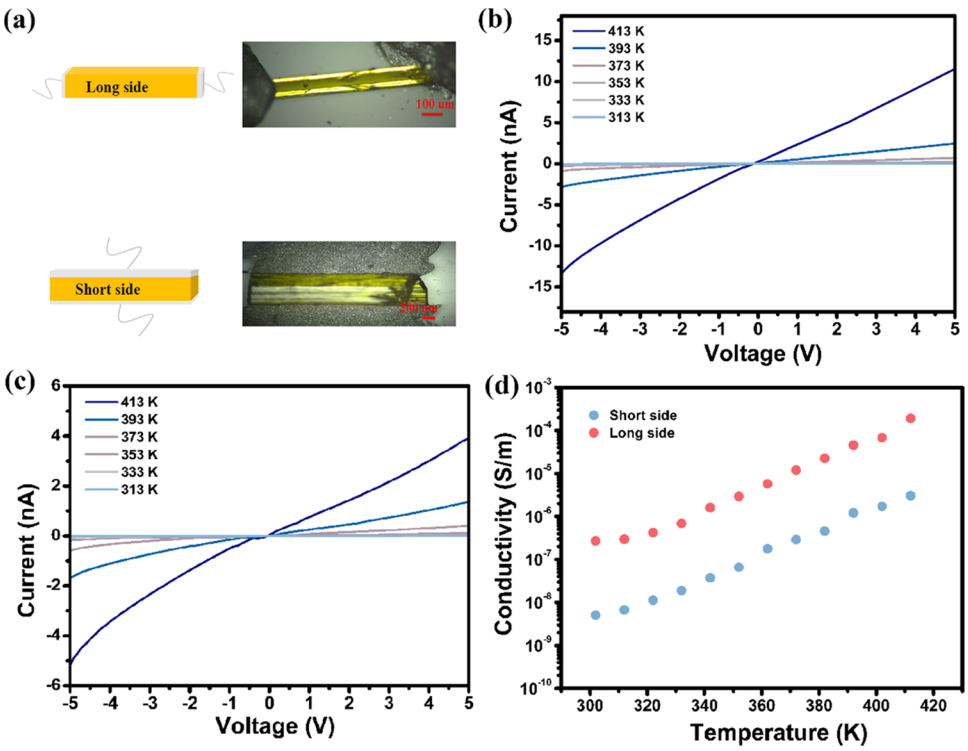

Figure 3. (a) Photograph of the single crystal of CuI-K-INA for anisotropic conductivity measurements by using a direct current two-terminal method. Scale bar, 100 μm (top right) and 200 μm (bottom right). Panels (b) and (c) are the temperature-dependent $I-V$ curves for CuI-K-INA along the long and short sides, respectively. (d) Temperature-dependent conductivity for CuI-K-INA along the long and short sides.

(*e.g.*, via K^+, INA, and its derivatives in this work) and consequently a much richer structural database with unique and new features.

Physical Characterizations. Compared with the wide band gap of CuI (E_a = 3.1 eV for γ-CuI, for instance), the blending of the K-INA-R and CuI offers a strong tunability to the electronic structures of the resulting hybrids, bringing their optical absorption edges well within the visible light region, ranging from ∼1.6 to ∼3.0 eV estimated from Tauc plots (Figures 2c and S17). To better understand their electronic structures, density functional theory (DFT) calculations were performed on all four title compounds. As depicted in Figures 2d,e and S18−S21, the valence band maximum (VBM) is composed primarily of the atomic orbitals of the inorganic motif (*i.e.*, Cu 3d and I 5p atomic orbitals), while the conduction band minimum (CBM) is contributed predominately from the organic ligands, specifically C, N, and O 2p orbitals for all of these compounds. Therefore, the organic ligands bearing different function groups play an important role not only in tailoring the dimensionality of CuI but also in tuning the band-gap, electronic, and optical properties of these hybrid compounds.[5] A comparative study of CuI-K-INA-NO_2 and CuI-K-INA (both with 2D-CuI layered modules) shows that the $-NO_2$ group with a strong electron-withdrawing ability in CuI-K-INA-NO_2 has lower CBM energies (Figure 2d,e); thus, its band gap (from both the experimental data and DFT result) is smaller than that of CuI-K-INA. The calculated band gaps of all four compounds are well in trend with the optical band gaps estimated from absorption experiments (Figures 2d,e and S18−S21) but with smaller values. Such underestimation is well documented and is caused mainly by the delocalization error of GGA functionals and the neglect of electron correlation effects.[10] For CuI-based hybrid materials, large deviations at a similar extent have been reported for a number of compounds.[9c,11] In addition, the Mott−Schottky test was performed on K-CuI-INA at 1000, 2000, and 3000 Hz (Figure S22). As shown in the Mott−Schottky plot, the C^{-2} value has a negative slope to the potential, while the intersection with the x-axis is independent of frequency. This result suggests that K-CuI-INA is a p-type semiconductor,[12] as previously found in a number of other CuI hybrid materials.[11a,13]

Interestingly, these compounds show structure-dependent photoconductivity under visible light irradiation, with magnitude ranging from 10^{-12} A to 10^{-7} A. CuI-K-INA-COOH and CuI-K-INA-OH with 1D-CuI chains exhibit comparatively low photoconduction with conductivity at a magnitude of 10^{-12} and 10^{-9} A, respectively (Figures S23 and S24). While for CuI-K-INA-NO_2 and CuI-K-INA with the extended 2D layered CuI modules, high photoconductivity at a magnitude of 10^{-8} and 10^{-7} A was achieved (Figure 2f). As p-type (primarily hole-conducting) semiconductors, their photoconductivity hinges largely on the valence bands, which are composed primarily of the orbitals of the inorganic modules. Therefore, the increase in the dimensionality of the CuI module from the 1D chain in CuI-K-INA-COOH and CuI-K-INA-OH to the 2D layer in K-INA-NO_2 and CuI-K-INA facilitates more delocalized conduction pathways and consequently enhances photoconductivity.[14] While K-INA-NO_2 has a narrower band gap, the bands are much more delocalized for CuI-K-INA, providing a more efficient conduction pathway and higher photoconductivity. However, one should realize that the influence of structural features, such as differences in the K-INA-R frameworks and coordination mode and strength between the atoms, cannot be ruled out.[15]

https://doi.org/10.1021/jacs.3c05095
J. Am. Chem. Soc. 2023, 145, 19293−19302

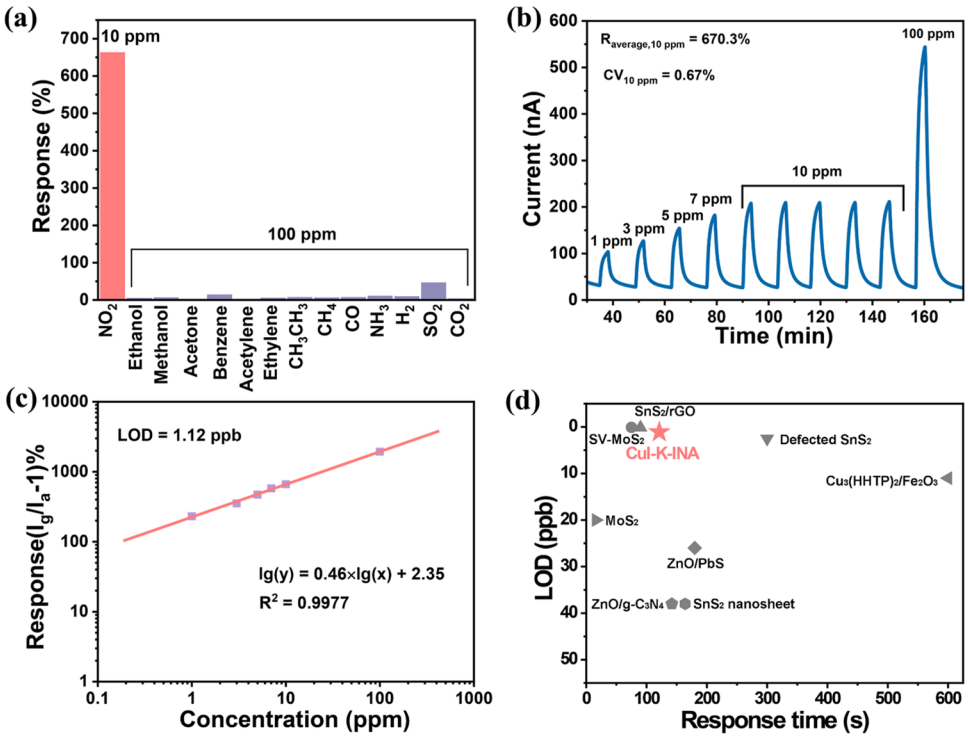

Figure 4. (a) Responses of CuI-K-INA as a sensor to 10 ppm NO_2 with other different 100 ppm gases. (b) Response and recovery curve of CuI-K-INA toward NO_2 with varied concentrations at RT under visible light irradiation. (c) Log−log linear fitting of the response−concentration plot. (d) Response time and LOD values of CuI-K-INA in comparison with the reported NO_2 sensors under visible light illumination.[20]

The anisotropic structural features in semiconductors make them attractive for optoelectronic applications.[16] As an example, CuI-K-INA, having a rodlike crystal morphology with millimeter (mm) sizes (Figure 3a), was selected to investigate the anisotropic semiconductive behavior. Single-crystal analysis indicates that the 2D inorganic CuI layer is parallel to the *bc* plane, and the *c* axis corresponds to the long direction of the rodlike crystal, while one short side of the crystal corresponds to the inorganic layered structure viewed along the *a* axis (Figures 2a and S25). The conductance of CuI-K-INA was measured using a direct current two-terminal method on a carefully selected single-crystal sample (Figure 3a). As shown in Figure 3b−d, the single crystal of CuI-K-INA exhibits a highly anisotropic charge transport behavior. At RT, the conductivity along the long side of the single crystal (within the 2D-CuI layer based on crystal structure analysis) is about two orders of magnitude higher than that measured along the short side (perpendicular to the 2D-CuI layer; Figure S26). Such a difference is understandable since the conductivity within the extended 2D inorganic network is significantly higher than that out of the 2D layer. Moreover, we carried out two-probe and four-probe measurements on a pressed pellet of CuI-K-INA. Conductivities at the same magnitude were obtained from the two experiments, indicating that the contact resistance had negligible influence on the anisotropic conductivity (Figure S27). The compound also shows a significant anisotropic temperature effect (Figure 3b,c). From RT to 413 K (140 °C), the conductivity of CuI-K-INA along the long side exhibits an increase of approximately three orders of magnitude, from 2.70×10^{-9} S/cm to 1.21×10^{-6} S/cm. The conductivity of CuI-K-INA crystal at 140 °C is lower than that of $Cu_2I_2(bse)_2$ bearing a selenium-bearing ligand ($\sigma = 2 \pm 1 \times 10^{-4}$ S/cm)[11b] but is comparable to that of $Cu_4I_6(bttmp)_2$ with $\sigma = 2.8 \times 10^{-6}$ S/cm.[13b] Furthermore, the conductivity of CuI-K-INA is 1−2 orders of magnitude higher than the reported values for hybrid perovskite single crystals, such as $MAPbI_3$ ($\sigma = 1 \times 10^{-8}$ S/cm), α-$FAPbI_3$ ($\sigma = 1.1 \times 10^{-7}$ S/cm), and $MAPbBr_3$ ($\sigma = 2 \times 10^{-8}$ S/cm),[17] measured using the same method. While along the short side, the conductivity also increases from 1.17×10^{-11} to 7.06×10^{-9} S/cm in the same temperature range (Figure 3d). The conductivity measured at lower temperatures (253−293 K) also exhibits a temperature-dependent increase (Figure S27). The results indicate a typical Arrhenius-type behavior and can be explained by charge transport arising from thermal activation conduction processes.[18]

In addition to the band-gap tunability due to tailored structures, these CuI-based hybrid structures also exhibit metal-to-ligand charge transfer (MLCT) and iodide-to-ligand charge transfer (XLCT) under photoexcitation, very similar to the previously reported CuI-bearing CPs and many CuI(L) (L = organic linker) hybrid structures;[19] except CuI-K-INA-NO_2, they all exhibit interestingly thermally activated delayed fluorescence (TADF) (Figures S28−S30). Taking CuI-K-INA for an example, it shows an orange emission maximized at 600 nm, with a decrease in fluorescence intensity and a blue shift when the temperature increases from 77 to 298 K (Figure S30). This result indicates that the optical characters observed in CuI(L) hybrid structures are inherited when CuI modules are confined in K-INA-R CPs. TG analysis of these compounds confirms their good thermal stabilities (stable up to 250−300 °C), which are comparable to those of the reported CuI-based hybrids modified with organic ligands (Figures S31−S34).[9c,19]

Gas Sensing Measurements. As depicted in Figures 4a and S37, different from the pristine CuI-based sensors that have low selectivity for NO_2, both CuI-K-INA-NO_2 and CuI-

https://doi.org/10.1021/jacs.3c05095
J. Am. Chem. Soc. 2023, 145, 19293−19302

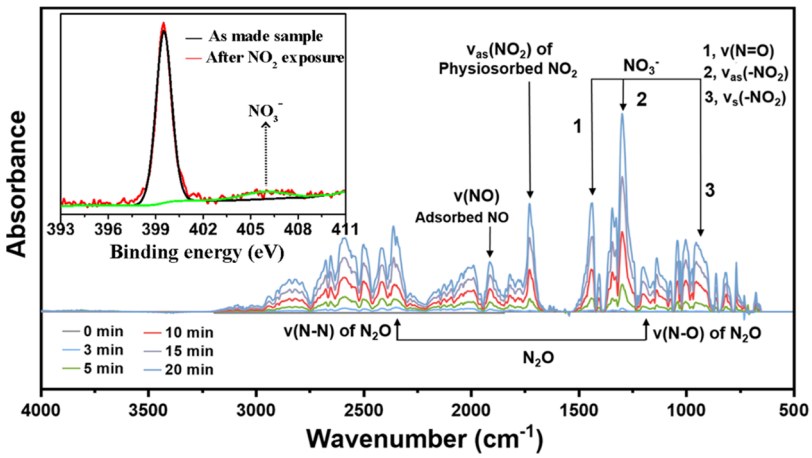

Figure 5. Time-resolved DRIFTS difference spectra of CuI-K-INA during NO_2 sensing. The inset is the XPS spectra of N 1s in CuI-K-INA before and after NO_2 exposure.

K-INA show high sensing selectivity toward NO_2 against other interference gas analytes at 100 ppm. As shown in Figures S38 and S39, CuI-K-INA-COOH and CuI-K-INA-OH, on the other hand, exhibit almost no chemiresistive sensing abilities toward NO_2 even at a high concentration of 100 ppm under the same experimental condition. The results are in accordance with their weak conductivity with low on/off ratios (Figures S23 and S24). As depicted in Figures S40 and S41, both CuI-K-INA-NO_2 and CuI-K-INA show a typical dynamic response-recovery behavior to a broad concentration range of NO_2 (1−100 ppm) at RT. Particularly, the conductance of CuI-K-INA shows an obvious increase upon exposure to NO_2 and then recovers back to the initial value when purged with dry air. The average response (R_{avg}) of five individually as-made devices toward 10 ppm NO_2 is up to 1434% for CuI-K-INA (Figure S40a). This value is ∼1.5 × 10^4 times higher than that of the pristine CuI (−0.0098% ppm^{-1}) toward per ppm NO_2 operated at an elevated temperature of 240 °C.[3b] The high response value and excellent selectivity indicate that confining CuI by the coordinating assembly is an efficient way to improve the gas sensing performances of the pristine CuX. The linear fitting of the plot deduces the limit of detection (LOD) of CuI-K-INA and CuI-K-INA-NO_2 to be 14.12 and 44.47 ppb, respectively, by setting the response to 10% (Figures S40b and S41c). The response and recovery times of CuI-K-INA toward 10 ppm NO_2 are 121.8 and 312.6 s, respectively (Figure S40c). The response value and LOD of CuI-K-INA measuring at the dark condition are comparable to those of the best sensor materials even working at high temperature (Table S2). As far as we are aware, both CuI-K-INA-NO_2 and CuI-K-INA represent the first CuI containing CP hybrid materials with a chemiresistive gas sensing ability. The cycling tests of CuI-K-INA and CuI-K-INA-NO_2 toward 10 ppm NO_2 reveal a comparably large coefficient of variation, indicating that the sensing repeatability can be improved.

The strong absorption of visible light of both compounds (Figure 2c) prompted us to investigate their sensing properties under light illumination. As seen in Figures 4b, S42, and S43, both CuI-K-INA-NO_2 and CuI-K-INA show an optimized NO_2 sensing performance compared with that without light irradiation. For CuI-K-INA-NO_2, the sensing coefficient of variation (CV) reduces to 5.8% under light irradiation toward high concentrations of 100 ppm NO_2, and the recovery time also decreases to 312.5 s (Figure S42), while for CuI-K-INA, the negligible CV value of 0.67% (decreased to 1/16 of that without light resistance; see Figure 4b) indicates its excellent sensing repeatability under light illumination. The LOD is decreased to 1.12 ppb, 12 times lower than that under dark operating conditions, which is superior to all previously reported NO_2 sensing materials working at RT and far below the NO_2 limit required by WHO (Figure 4c).[20] The recovery time is further shortened to 212.3 s (Figure S43). The enhancement in sensitivity and reduced recovery time under light illumination are similar to those observed in graphene-based NO_2 sensors, such as graphene with monodisperse polymer beads and g-C_3N_4/graphene.[21] However, it surpasses the performance of transition-metal dichalcogenides (e.g., MoS_2, SnS_2) and their complex materials (e.g., SnS_2/graphene).[20c−e,22] Taking into consideration the recovery capability, response time, and LOD value, CuI-K-INA stands out as one of the best chemiresistive NO_2 sensors (Figure 4d), comparable to the best inorganic sensors including semiconductors and hybrids operating at RT under light illumination (Table S3).

Mechanism Studies. Generally, the as-made CuI-K-INA sample was ground into a fine powder, which was then suspended in a solvent and drip-coated onto the interdigital electrode to fabricate a sensing device for performance investigation (Figure S35). Initially, the BET surface area of the powdered CuI-K-INA sample was measured and showed no N_2 adsorption, consistent with its nonporous structure (Figure S44). This further confirms that the chemiresistive response to NO_2 does not arise from bulk absorption into the crystalline structure. Time-resolved diffuse reflectance infrared Fourier transform spectroscopy (DRIFTS) measurement of CuI-K-INA has been conducted to understand the NO_2 sensing mechanism. As shown in Figure 5, compared with DRIFTS for the pristine CuI-K-INA (Figure S45), a series of new bands have been observed after the sample exposing to NO_2 and the intensities of the new peaks show continuous increase along with the accumulation of exposure time. Gas-phase NO_2 can be seen around 1620 and 1260 cm^{-1}, which are assigned to its asymmetric and symmetric stretching modes ($\nu_{as,s}$).[23] Molecularly adsorbed NO_2 was also detected by observing its ν_{as} band at 1710 cm^{-1}, which shifted upward (blue-) with respect to the value of gas phase due to partial electron donation to the surface that stiffens the N═O bond.[24] Three new features labeled as 1, 2, and 3 in Figure 5 are the

https://doi.org/10.1021/jacs.3c05095
J. Am. Chem. Soc. 2023, 145, 19293−19302

characteristic bands of nitrate species (NO_3^-) that are ascribed to the N═O stretching and the asymmetric and symmetric stretching vibrations of $-NO_2$ within NO_3^- ions.[25] The large separation between 1 and 2 over 180 cm^{-1} indicates the formation of bridging or chelating nitrate complex on the particle surface through bidentate bonding configuration.[25a] Besides, NO and N_2O species were also generated during the sensing process as indicated by the DRIFTS. NO is characterized by the broad band around 1800−1900 cm^{-1}, which corresponds to its stretching vibration of nitrosyl species formed on the cationic sites,[24e] and N_2O is characterized by N═N and N−O stretching modes around 2400−2300 and 1300−1200 cm^{-1}, respectively. The determination of the exact positions for these bands is obscured by the perturbation of CP phonon modes, i.e., the derivative-like features, occurring in these regions (see Figure S45). Nevertheless, they grow in a proportional manner with NO_3^- bands, indicating that they are the reaction products of NO_2 with CuI-K-INA.

To further investigate the sensing mechanism, EPR and XPS measurements were also performed. As seen in Figure S46, the EPR spectrum of CuI-K-INA exposing to NO_2 shows an obvious signal at g = 2.06, corresponding to the characteristic signal of the metal center Cu^{2+} compared with that of the pristine sample.[26] This result further indicates that the 2D-CuI modules confined in CuI-K-INA are the sensing sites. The XPS measurements were further performed on the NO_2-exposed CuI-K-INA sample, and both the characteristic peaks of Cu-2p and I-3d remained unchanged (Figure S47), suggesting that the interaction between NO_2 and CuI-K-INA might be a reversible charge-transfer interactions that was in accordance with the former reports.[26] However, the N 1s shows a small shoulder peak at 406.0 eV after exposing to NO_2, which is the typical position of NO_3^- ions on material surfaces[25b] and is consistent with the DRIFTS result (inset in Figure 5). The NO_2 sensing process would be viewed as a Lewis acid−base interaction between the Cu(I) and NO_2, which catalyzes the disproportionation reaction for NO_2

$$2NO_2(ads) \rightarrow NO_3^-(ads) + NO(gas) + N_2O(gas)$$

The highly acidic NO_2 extracts electrons from Cu(I) by forming a comparatively strong interaction with Cu(I)-N-nitro[20h,27] and then results in the resistance change. It is widely acknowledged that the sensing response is a complex process that involves a synergistic effect between the sensing material and the target gas species, in addition to efficient light absorption.[28] Based on UV−vis spectroscopy and electronic structure analysis, electron−hole pairs in K-CuI-INA can be effectively separated under visible light illumination. Excited electrons in K-CuI-INA transit from the valence band to the conduction band, resulting in an increase in electron concentration. As a strong oxidizer, the adsorbed NO_2 is able to extract electrons from the surface of the hybrid compound under light illumination, thereby enhancing the sensing sensitivity. Furthermore, the additional excited holes accelerate the physical desorption of NO_2 by decomposing the negatively charged NO_2 δ- species.[20e,29] As a result, the desorption rate exceeds the adsorption rate, leading to a shortened recovery time under light activation.

■ CONCLUSIONS

In summary, we have demonstrated that the extended 1D and 2D structures of CuI modules can be confined into K-INA-R CPs by the coordination assembly to form a series of semiconducting hybrid compounds. The dimensionality and structure of the inorganic module can be tailored by tuning the coordination modes between metals and ligands with varied coordination sites. Remarkably, these compounds represent the first CuI-bearing hybrid-based gas sensors toward NO_2, and the sensing performances are comparable to the best present chemiresistors. Many characterizations coupled with theoretical calculations are applied to reveal their structure−property relationship. This work provides a new approach to designing custom-tailored functional hybrids, not only with novel structure features but also with tunable properties by confining functional (magnetic, ferroelectric, catalytic, etc.) inorganic modules into coordination polymers.

■ ASSOCIATED CONTENT

Supporting Information

The Supporting Information is available free of charge at https://pubs.acs.org/doi/10.1021/jacs.3c05095.

Experimental details, more structural details and figures, powder X-ray diffraction patterns, TG, UV−vis spectra, and semiconducting characterizations, and gas sensing measurements (PDF)

Accession Codes

CCDC 2252166−2252169 contain the supplementary crystallographic data for this paper. These data can be obtained free of charge via www.ccdc.cam.ac.uk/data_request/cif, or by emailing data_request@ccdc.cam.ac.uk, or by contacting The Cambridge Crystallographic Data Centre, 12 Union Road, Cambridge CB2 1EZ, UK; fax: +44 1223 336033.

■ AUTHOR INFORMATION

Corresponding Authors

Xingwu Liu − *Synfuels China Technology Co.Ltd., Beijing 101407, P. R. China;* orcid.org/0000-0002-8564-1151; Email: liuxingwu@sxicc.ac.cn

Gang Xu − *State Key Laboratory of Structural Chemistry, Fujian Provincial Key Laboratory of Materials and Techniques toward Hydrogen Energy, Fujian Institute of Research on the Structure of Matter, the Chinese Academy of Sciences, Fuzhou, Fujian 350002, P. R. China;* orcid.org/0000-0001-8562-0724; Email: gxu@fjirsm.ac.cn

Jing Li − *Department of Chemistry and Chemical Biology, Rutgers University, New Brunswick, New Jersey 08854, United States;* orcid.org/0000-0001-7792-4322; Email: jingli@rutgers.edu

Authors

Zhao-Feng Wu − *Department of Chemistry and Chemical Biology, Rutgers University, New Brunswick, New Jersey 08854, United States; State Key Laboratory of Structural Chemistry, Fujian Provincial Key Laboratory of Materials and Techniques toward Hydrogen Energy, Fujian Institute of Research on the Structure of Matter, the Chinese Academy of Sciences, Fuzhou, Fujian 350002, P. R. China; Fujian Science & Technology Innovation Laboratory for Optoelectronic Information of China, Fuzhou, Fujian 350108, P. R. China*

Chuanzhe Wang − *State Key Laboratory of Structural Chemistry, Fujian Provincial Key Laboratory of Materials and Techniques toward Hydrogen Energy, Fujian Institute of Research on the Structure of Matter, the Chinese Academy of Sciences, Fuzhou, Fujian 350002, P. R. China*

https://doi.org/10.1021/jacs.3c05095
J. Am. Chem. Soc. 2023, 145, 19293−19302

Kui Tan − *Department of Chemistry, University of North Texas, Denton, Texas 76203, United States;* orcid.org/0000-0002-5167-7295

Zhihua Fu − *State Key Laboratory of Structural Chemistry, Fujian Provincial Key Laboratory of Materials and Techniques toward Hydrogen Energy, Fujian Institute of Research on the Structure of Matter, the Chinese Academy of Sciences, Fuzhou, Fujian 350002, P. R. China*

Simon J. Teat − *Advanced Light Source, Lawrence Berkeley National Laboratory, Berkeley, California 94720, United States*

Zi-Wei Li − *State Key Laboratory of Structural Chemistry, Fujian Provincial Key Laboratory of Materials and Techniques toward Hydrogen Energy, Fujian Institute of Research on the Structure of Matter, the Chinese Academy of Sciences, Fuzhou, Fujian 350002, P. R. China; Fujian Science & Technology Innovation Laboratory for Optoelectronic Information of China, Fuzhou, Fujian 350108, P. R. China*

Xiuze Hei − *Department of Chemistry and Chemical Biology, Rutgers University, New Brunswick, New Jersey 08854, United States*

Xiao-Ying Huang − *State Key Laboratory of Structural Chemistry, Fujian Provincial Key Laboratory of Materials and Techniques toward Hydrogen Energy, Fujian Institute of Research on the Structure of Matter, the Chinese Academy of Sciences, Fuzhou, Fujian 350002, P. R. China;* orcid.org/0000-0002-3514-216X

Complete contact information is available at: https://pubs.acs.org/10.1021/jacs.3c05095

Author Contributions

∇

Z.-F.W. and C.W.contributed equally to this work.

Funding

The authors thank the partial support from the U.S. Department of Energy, Office of Science, Office of Basic Energy Sciences under Award No. DE-SC0019902. This research used resources from the Advanced Light Source (ALS), which is a DOE Office of Science User Facility under contract DE-AC02-05CH11231. The team in FJIRSM acknowledges the support from the National Natural Science Foundation of China (Nos. 22175178, 91961115, 22171263), the Scientific Research and Equipment Development Project of CAS (YJKYQ20210024), the Fujian Science AND Technology Innovation Laboratory for Optoelectronic Information of China (2021ZR130 and 2021ZR101), and the Natural Science Foundation of Fujian Province (2021J02017).

Notes

The authors declare no competing financial interest.

■ ACKNOWLEDGMENTS

The authors are grateful to Dr. Liang-Xiao Tan (Beijing Institute of Technology, P. R. China) for his help in designing the scheme and TOC figures; the authors also thank Ji-Long Li (Fuzhou University) for helping with EPR measurements.

■ REFERENCES

(1) (a) Grundmann, M.; Schein, F. L.; Lorenz, M.; Bontgen, T.; Lenzner, J.; von Wenckstern, H. Cuprous iodide - a p-type transparent semiconductor: history and novel applications. *Phys. Status Solidi A* **2013**, *210*, 1671−1703. (b) Gong, C.; Chu, J.; Yin, C.; Yan, C.; Hu, X.; Qian, S.; Hu, Y.; Hu, K.; Huang, J.; Wang, H.; Wang, Y.; Wangyang, P.; Lei, T.; Dai, L.; Wu, C.; Chen, B.; Li, C.; Liao, M.; Zhai, T.; Xiong, J. Self-Confined Growth of Ultrathin 2D Nonlayered Wide-Bandgap Semiconductor CuBr Flakes. *Adv. Mater.* **2019**, *31*, No. e1903580. (c) Guo, Z.; Li, J.; Pan, R.; Cheng, J.; Chen, R.; He, T. All-inorganic copper(i)-based ternary metal halides: promising materials toward optoelectronics. *Nanoscale* **2020**, *12*, 15560−15576. (d) Yamada, N.; Tanida, Y.; Murata, H.; Kondo, T.; Yoshida, S. Wide-Range-Tunable p-Type Conductivity of Transparent $CuI_{1-x}Br_x$ Alloy. *Adv. Funct. Mater.* **2020**, *30*, No. 2003096. (e) Li, Y. Y.; Zhou, Z. C.; Tewari, N.; Ng, M.; Geng, P.; Chen, D. Z.; Ko, P. K.; Qammar, M.; Guo, L.; Halpert, J. E. Progress in copper metal halides for optoelectronic applications. *Mater. Chem. Front.* **2021**, *5*, 4796−4820. (f) Liu, A.; Zhu, H.; Kim, M. G.; Kim, J.; Noh, Y. Y. Engineering Copper Iodide (CuI) for Multifunctional p-Type Transparent Semiconductors and Conductors. *Adv. Sci.* **2021**, *8*, No. 2100546.

(2) (a) Zhang, Y.; Xu, P.; Xu, J.; Li, H.; Ma, W. NH_3 Sensing Mechanism Investigation of CuBr: Different Complex Interactions of the Cu^+ Ion with NH_3 and O_2 Molecules. *J. Phys. Chem. C* **2011**, *115*, 2014−2019. (b) Güntner, A. T.; Wied, M.; Pineau, N. J.; Pratsinis, S. E. Rapid and Selective NH_3 Sensing by Porous CuBr. *Adv. Sci.* **2020**, *7*, No. 1903390. (c) Kim, S.-K.; Yu, B.-H.; Na, C. W.; Lee, J.-H.; Yoon, J.-W. Facile and rapid fabrication of porous CuBr films by solution oxidation and their application for the exclusive detection of NH_3 at room temperature. *J. Mater. Chem. A* **2022**, *10*, 950−959.

(3) (a) Wolpert, B.; Leitl, M.; Pfitzner, A.; Mirsky, V. M. Chemosensitive properties of electrically conductive Cu(I) compounds at room temperature. *Sens. Actuators, B* **2008**, *134*, 839−842. (b) Wolpert, B.; Wolfbeis, O. S.; Mirsky, V. M. Gas sensing properties of electrically conductive Cu(I) compounds at elevated temperatures. *Sens. Actuators, B* **2009**, *142*, 446−450.

(4) (a) Stetter, J. R.; Li, J. Amperometric gas sensors–a review. *Chem. Rev.* **2008**, *108*, 352−366. (b) Gallington, L. C.; Kim, I. S.; Liu, W. G.; Yakovenko, A. A.; Platero-Prats, A. E.; Li, Z.; Wang, T. C.; Hupp, J. T.; Farha, O. K.; Truhlar, D. G.; Martinson, A. B. F.; Chapman, K. W. Regioselective Atomic Layer Deposition in Metal-Organic Frameworks Directed by Dispersion Interactions. *J. Am. Chem. Soc.* **2016**, *138*, 13513−13516. (c) Wang, X. N.; Zhang, P.; Kirchon, A.; Li, J. L.; Chen, W. M.; Zhao, Y. M.; Li, B.; Zhou, H. C. Crystallographic Visualization of Postsynthetic Nickel Clusters into Metal-Organic Framework. *J. Am. Chem. Soc.* **2019**, *141*, 13654−13663. (d) Gonzalez, M. I.; Turkiewicz, A. B.; Darago, L. E.; Oktawiec, J.; Bustillo, K.; Grandjean, F.; Long, G. J.; Long, J. R. Confinement of atomically defined metal halide sheets in a metal-organic framework. *Nature* **2020**, *577*, 64−68.

(5) (a) Peng, R.; Li, M.; Li, D. Copper(I) halides: A versatile family in coordination chemistry and crystal engineering. *Coord. Chem. Rev.* **2010**, *254*, 1−18. (b) Liu, W.; Fang, Y.; Li, J. Copper Iodide Based Hybrid Phosphors for Energy-Efficient General Lighting Technologies. *Adv. Funct. Mater.* **2018**, *28*, No. 1705593. (c) Troyano, J.; Zamora, F.; Delgado, S. Copper(i)-iodide cluster structures as functional and processable platform materials. *Chem. Soc. Rev.* **2021**, *50*, 4606−4628.

(6) (a) Christians, J. A.; Fung, R. C.; Kamat, P. V. An inorganic hole conductor for organo-lead halide perovskite solar cells. Improved hole conductivity with copper iodide. *J. Am. Chem. Soc.* **2014**, *136*, 758−764. (b) Sepalage, G. A.; Meyer, S.; Pascoe, A.; Scully, A. D.; Huang, F. Z.; Bach, U.; Cheng, Y. B.; Spiccia, L. Copper(I) Iodide as Hole-Conductor in Planar Perovskite Solar Cells: Probing the Origin of J-V Hysteresis. *Adv. Funct. Mater.* **2015**, *25*, 5650−5661. (c) Liu, A.; Zhu, H.; Park, W. T.; Kang, S. J.; Xu, Y.; Kim, M. G.; Noh, Y. Y. Room-Temperature Solution-Synthesized p-Type Copper(I) Iodide Semiconductors for Transparent Thin-Film Transistors and Complementary Electronics. *Adv. Mater.* **2018**, *30*, No. e1802379. (d) Koyasu, S.; Miyauchi, M. Recent Research Trends in Point Defects in Copper Iodide Semiconductors. *J. Electron. Mater.* **2020**, *49*, 907−909.

(7) (a) Gu, X.; Xue, D. 3D coordination framework $[Ln_4(\mu_3\text{-}OH)_2Cu_6I_5(IN)_8(OAc)_3]$ (IN = isonicotinate): employing 2D layers of lanthanide wheel clusters and 1D chains of copper halide clusters.

Inorg. Chem. **2007**, *46*, 5349−5353. (b) Fan, L. Q.; Chen, Y.; Wu, J. H.; Huang, Y. F. Hydrothermal Synthesis, Crystal Structure and Characterization of a Novel 3D Pillared-Layer 3d-4f Lanthanum-Copper Heterometallic Coordination Polymer. *J. Inorg. Organomet. Polym. Mater.* **2011**, *21*, 346−351. (c) Zeng, R. H.; Peng, G.; Qiu, Y. C.; Zheng, S. R.; Li, W. S.; Zhang, W. X.; Deng, H.; Cai, Y. P. Synthesis, crystal structures and properties of Ln(III)-Cu(I)-Na(I) and Ln(III)-Ag(I) heterometallic coordination polymers. *CrystEngComm* **2011**, *13*, 3910−3919. (d) Fang, W. H.; Yang, G. Y. Three pillared-layer 3d-4f heterometallic frameworks based on tetranuclear lanthanide clusters. *CrystEngComm* **2013**, *15*, 9504−9512. (e) Fang, W. H.; Yang, G. Y. Constructing heterometallic frameworks with highly connected topology based on edge-to-edge hexanuclear lanthanide clusters. *CrystEngComm* **2014**, *16*, 1885−1892.

(8) (a) Cariati, E.; Bu, X.; Ford, P. C. Solvent- and Vapor-Induced Isomerization between the Luminescent Solids $[CuI(4\text{-pic})]_4$ and $[CuI(4\text{-pic})]_\infty$ (pic = methylpyridine). The Structural Basis for the Observed Luminescence Vapochromism. *Chem. Mater.* **2000**, *12*, 3385−3391. (b) Cariati, E.; Roberto, D.; Ugo, R.; Ford, P. C.; Galli, S.; Sironi, A. New structural motifs, unusual quenching of the emission, and second harmonic generation of copper(I) iodide polymeric or oligomeric adducts with para-substituted pyridines or trans-stilbazoles. *Inorg. Chem.* **2005**, *44*, 4077−4085.

(9) (a) Liu, W.; Fang, Y.; Wei, G. Z.; Teat, S. J.; Xiong, K.; Hu, Z.; Lustig, W. P.; Li, J. A Family of Highly Efficient CuI-Based Lighting Phosphors Prepared by a Systematic, Bottom-up Synthetic Approach. *J. Am. Chem. Soc.* **2015**, *137*, 9400−9408. (b) Artem'ev, A. V.; Davydova, M. P.; Hei, X.; Rakhmanova, M. I.; Samsonenko, D. G.; Bagryanskaya, I. Y.; Brylev, K. A.; Fedin, V. P.; Chen, J.-S.; Cotlet, M.; Li, J. Family of Robust and Strongly Luminescent CuI-Based Hybrid Networks Made of Ionic and Dative Bonds. *Chem. Mater.* **2020**, *32*, 10708−10718. (c) Hei, X.; Liu, W.; Zhu, K.; Teat, S. J.; Jensen, S.; Li, M.; O'Carroll, D. M.; Wei, K.; Tan, K.; Cotlet, M.; Thonhauser, T.; Li, J. Blending Ionic and Coordinate Bonds in Hybrid Semiconductor Materials: A General Approach toward Robust and Solution-Processable Covalent/Coordinate Network Structures. *J. Am. Chem. Soc.* **2020**, *142*, 4242−4253.

(10) (a) Mori-Sánchez, P.; Cohen, A. J.; Yang, W. Localization and delocalization errors in density functional theory and implications for band-gap prediction. *Phys. Rev. Lett.* **2008**, *100*, No. 146401. (b) Zheng, X.; Cohen, A. J.; Mori-Sanchez, P.; Hu, X.; Yang, W. Improving band gap prediction in density functional theory from molecules to solids. *Phys. Rev. Lett.* **2011**, *107*, No. 026403. (c) Cohen, A. J.; Mori-Sanchez, P.; Yang, W. Challenges for density functional theory. *Chem. Rev.* **2012**, *112*, 289−320.

(11) (a) Huang, X.; Qiu, Y.; Wang, Y.; Liu, L.; Wu, X.; Liang, Y.; Cui, Y.; Sun, Y.; Zou, Y.; Zhu, J.; Fang, W.; Sun, J.; Xu, W.; Zhu, D. Highly Conducting Organic-Inorganic Hybrid Copper Sulfides $Cu_xC_6S_6$ (x=4 or 5.5): Ligand-Based Oxidation-Induced Chemical and Electronic Structure Modulation. *Angew. Chem., Int. Ed.* **2020**, *59*, 22602−22609. (b) Li, J.; Fang, Y.; Zhu, K.; Teat, S. J.; Reid, O. G.; Hei, X. Z.; Zhu, K.; Fang, X. C.; Li, M. X.; Sojdak, C. A.; Cotlet, M. Robust and Highly Conductive Water-Stable Copper Iodide-Based Hybrid Single Crystals. *Chem. Mater.* **2022**, *34*, 10040−10049. (c) Hei, X. Z.; Zhu, K.; Carignan, G.; Teat, S. J.; Li, M. X.; Zhang, G. Y.; Bonite, M.; Li, J. Solution-processable copper(I) iodide-based inorganic-organic hybrid semiconductors composed of both coordinate and ionic bonds. *J. Solid State Chem.* **2022**, *314*, No. 123427. (d) Artem'ev, A. V.; Doronina, E. P.; Rakhmanova, M. I.; Hei, X.; Stass, D. V.; Tarasova, O. A.; Bagryanskaya, I. Y.; Samsonenko, D. G.; Novikov, A. S.; Nedolya, N. A.; Li, J. A family of CuI-based 1D polymers showing colorful short-lived TADF and phosphorescence induced by photo- and X-ray irradiation. *Dalton Trans.* **2023**, *52*, 4017−4027.

(12) (a) Liu, L.; Du, S.; Guo, X.; Xiao, Y.; Yin, Z.; Yang, N.; Bao, Y.; Zhu, X.; Jin, S.; Feng, Z.; Zhang, F. Water-Stable Nickel Metal-Organic Framework Nanobelts for Cocatalyst-Free Photocatalytic Water Splitting to Produce Hydrogen. *J. Am. Chem. Soc.* **2022**, *144*, 2747−2754. (b) Zhou, X. C.; Liu, C.; Su, J.; Liu, Y. F.; Mu, Z.; Sun, Y.; Yang, Z. M.; Yuan, S.; Ding, M.; Zuo, J. L. Redox-Active Mixed-Linker Metal-Organic Frameworks with Switchable Semiconductive Characteristics for Tailorable Chemiresistive Sensing. *Angew. Chem., Int. Ed.* **2023**, *62*, No. e202211850.

(13) (a) Ki, W.; Hei, X. Z.; Yi, H. T.; Liu, W.; Teat, S. J.; Li, M. J.; Fang, Y.; Podzorov, V.; Garfunkel, E.; Li, J. Two-Dimensional Copper Iodide-Based Inorganic-Organic Hybrid Semiconductors: Synthesis, Structures, and Optical and Transport Properties. *Chem. Mater.* **2021**, *33*, 5317−5325. (b) Zhu, K.; Cheng, Z. K.; Rangan, S.; Cotlet, M.; Du, J. B.; Kasaei, L.; Teat, S. J.; Liu, W.; Chen, Y. F.; Feldman, L. C.; O'Carroll, D. M.; Li, J. A New Type of Hybrid Copper Iodide as Nontoxic and Ultrastable LED Emissive Layer Material. *ACS Energy Lett.* **2021**, *6*, 2565−2574.

(14) (a) Mohammadpour, A.; Farsinezhad, S.; Wiltshire, B. D.; Shankar, K. Majority carrier transport in single crystal rutile nanowire arrays. *Phys. Status Solidi RRL* **2014**, *8*, 512−516. (b) Wang, S.; Kitao, T.; Guillou, N.; Wahiduzzaman, M.; Martineau-Corcos, C.; Nouar, F.; Tissot, A.; Binet, L.; Ramsahye, N.; Devautour-Vinot, S.; Kitagawa, S.; Seki, S.; Tsutsui, Y.; Briois, V.; Steunou, N.; Maurin, G.; Uemura, T.; Serre, C. A phase transformable ultrastable titanium-carboxylate framework for photoconduction. *Nat. Commun.* **2018**, *9*, No. 1660.

(15) (a) Knutson, J. L.; Martin, J. D.; Mitzi, D. B. Tuning the band gap in hybrid tin iodide perovskite semiconductors using structural templating. *Inorg. Chem.* **2005**, *44*, 4699−4705. (b) Takahashi, Y.; Obara, R.; Nakagawa, K.; Nakano, M.; Tokita, J. Y.; Inabe, T. Tunable charge transport in soluble organic-inorganic hybrid semiconductors. *Chem. Mater.* **2007**, *19*, 6312−6316. (c) Choi, W. S.; Chisholm, M. F.; Singh, D. J.; Choi, T.; Jellison, G. E., Jr; Lee, H. N. Wide bandgap tunability in complex transition metal oxides by site-specific substitution. *Nat. Commun.* **2012**, *3*, No. 689. (d) Filip, M. R.; Eperon, G. E.; Snaith, H. J.; Giustino, F. Steric engineering of metal-halide perovskites with tunable optical band gaps. *Nat. Commun.* **2014**, *5*, No. 5757.

(16) (a) Larson, B. E.; Ehrenreich, H. Anisotropic superexchange and spin-resonance linewidth in diluted magnetic semiconductors. *Phys. Rev. B* **1989**, *39*, 1747−1759. (b) Sharma, A.; Yan, H.; Zhang, L.; Sun, X.; Liu, B.; Lu, Y. Highly Enhanced Many-Body Interactions in Anisotropic 2D Semiconductors. *Acc. Chem. Res.* **2018**, *51*, 1164−1173. (c) Li, X.; Liu, H. Y.; Ke, C. M.; Tang, W. Q.; Liu, M. Y.; Huang, F. H.; Wu, Y. P.; Wu, Z. M.; Kang, J. Y. Review of Anisotropic 2D Materials: Controlled Growth, Optical Anisotropy Modulation, and Photonic Applications. *Laser Photonics Rev.* **2021**, *15*, No. 2100322. (d) Wei, L. B.; Li, Y. R.; Tian, C. F.; Jiang, J. Recent Progress in Anisotropic 2D Semiconductors: From Material Properties to Photoelectric Detection. *Phys. Status Solidi A* **2021**, *218*, No. 2100204.

(17) (a) Saidaminov, M. I.; Adinolfi, V.; Comin, R.; Abdelhady, A. L.; Peng, W.; Dursun, I.; Yuan, M.; Hoogland, S.; Sargent, E. H.; Bakr, O. M. Planar-integrated single-crystalline perovskite photodetectors. *Nat. Commun.* **2015**, *6*, No. 8724. (b) Shi, D.; Adinolfi, V.; Comin, R.; Yuan, M.; Alarousu, E.; Buin, A.; Chen, Y.; Hoogland, S.; Rothenberger, A.; Katsiev, K.; Losovyj, Y.; Zhang, X.; Dowben, P. A.; Mohammed, O. F.; Sargent, E. H.; Bakr, O. M. Low trap-state density and long carrier diffusion in organolead trihalide perovskite single crystals. *Science* **2015**, *347*, 519−522. (c) Han, Q.; Bae, S. H.; Sun, P.; Hsieh, Y. T.; Yang, Y. M.; Rim, Y. S.; Zhao, H.; Chen, Q.; Shi, W.; Li, G.; Yang, Y. Single Crystal Formamidinium Lead Iodide ($FAPbI_3$): Insight into the Structural, Optical, and Electrical Properties. *Adv. Mater.* **2016**, *28*, 2253−2258.

(18) (a) Huang, Y. L.; Chiu, S. P.; Zhu, Z. X.; Li, Z. Q.; Lin, J. J. Variable-range-hopping conduction processes in oxygen deficient polycrystalline ZnO films. *J. Appl. Phys.* **2010**, *107*, No. 063715. (b) Tarun, M. C.; McCluskey, M. D. Infrared absorption of hydrogen-related defects in strontium titanate. *J. Appl. Phys.* **2011**, *109*, No. 063706.

(19) (a) Vitale, M. Luminescent mixed ligand copper(I) clusters $(CuI)_n(L)_m$ (L=pyridine, piperidine): thermodynamic control of molecular and supramolecular species. *Coord. Chem. Rev.* **2001**, *219-221*, 3−16. (b) Czerwieniec, R.; Leitl, M. J.; Homeier, H. H. H.;

https://doi.org/10.1021/jacs.3c05095
J. Am. Chem. Soc. 2023, 145, 19293−19302

Yersin, H. Cu(I) complexes - Thermally activated delayed fluorescence. Photophysical approach and material design. *Coord. Chem. Rev.* **2016**, *325*, 2−28. (c) Fang, Y.; Liu, W.; Teat, S. J.; Dey, G.; Shen, Z. Q.; An, L. T.; Yu, D. C.; Wang, L.; O'Carroll, D. M.; Li, J. A Systematic Approach to Achieving High Performance Hybrid Lighting Phosphors with Excellent Thermal- and Photostability. *Adv. Funct. Mater.* **2017**, *27*, No. 1603444. (d) Liu, W.; Zhu, K.; Teat, S. J.; Dey, G.; Shen, Z.; Wang, L.; O'Carroll, D. M.; Li, J. All-in-One: Achieving Robust, Strongly Luminescent and Highly Dispersible Hybrid Materials by Combining Ionic and Coordinate Bonds in Molecular Crystals. *J. Am. Chem. Soc.* **2017**, *139*, 9281−9290. (e) Hei, X.; Li, J. All-in-one: a new approach toward robust and solution-processable copper halide hybrid semiconductors by integrating covalent, coordinate and ionic bonds in their structures. *Chem. Sci.* **2021**, *12*, 3805−3817. (f) Hei, X. Z.; Teat, S. J.; Li, M. X.; Bonite, M.; Li, J. Highly soluble copper(i) iodide-based hybrid luminescent semiconductors containing molecular and one-dimensional coordinated anionic inorganic motifs. *J. Mater. Chem. C* **2023**, *11*, 3086−3094.

(20) (a) Chen, R.; Wang, J.; Xia, Y.; Xiang, L. Near infrared light enhanced room-temperature NO_2 gas sensing by hierarchical ZnO nanorods functionalized with PbS quantum dots. *Sens. Actuators, B* **2018**, *255*, 2538−2545. (b) Guo, J.; Wen, R.; Zhai, J.; Wang, Z. L. Enhanced NO_2 gas sensing of a single-layer MoS_2 by photogating and piezo-phototronic effects. *Sci. Bull.* **2019**, *64*, 128−135. (c) Huang, Y. F.; Jiao, W. C.; Chu, Z. M.; Ding, G. M.; Yan, M. L.; Zhong, X.; Wang, R. G. Ultrasensitive room temperature ppb-level NO_2 gas sensors based on SnS_2/rGO nanohybrids with P-N transition and optoelectronic visible light enhancement performance. *J. Mater. Chem. C* **2019**, *7*, 8616−8625. (d) Yan, W. J.; Chen, D. Y.; Fuh, H. R.; Li, Y. L.; Zhang, D.; Liu, H.; Wu, G.; Zhang, L.; Ren, X.; Cho, J.; Choi, M.; Chun, B. S.; Coileain, C. O.; Xu, H. J.; Wang, Z.; Jiang, Z.; Chang, C. R.; Wu, H. C. Photo-enhanced gas sensing of SnS_2 with nanoscale defects. *RSC Adv.* **2019**, *9*, 626−635. (e) Gu, D.; Wang, X. Y.; Liu, W.; Li, X. G.; Lin, S. W.; Wang, J.; Rumyantseva, M. N.; Gaskov, A. M.; Akbar, S. A. Visible-light activated room temperature NO_2 sensing of SnS_2 nanosheets based chemiresistive sensors. *Sens. Actuators, B* **2020**, *305*, No. 127455. (f) Wang, H. T.; Bai, J. H.; Dai, M.; Liu, K. P.; Liu, Y. Y.; Zhou, L. S.; Liu, F. M.; Liu, F. M.; Gao, Y.; Yan, X.; Lu, G. Y. Visible light activated excellent NO_2 sensing based on 2D/2D ZnO/g-C_3N_4 heterojunction composites. *Sens. Actuators, B* **2020**, *304*, No. 127287. (g) Xia, Y.; Hu, C. Y.; Guo, S. H.; Zhang, L. B.; Wang, M. J.; Peng, J. H.; Xu, L.; Wang, J. Sulfur-Vacancy-Enriched MoS_2 Nanosheets Based Heterostructures for Near-Infrared Optoelectronic NO_2 Sensing. *ACS Appl. Nano Mater.* **2020**, *3*, 665−673. (h) Jo, Y. M.; Lim, K.; Yoon, J. W.; Jo, Y. K.; Moon, Y. K.; Jang, H. W.; Lee, J. H. Visible-Light-Activated Type II Heterojunction in Cu_3(hexahydroxytriphenylene)$_2$/Fe_2O_3 Hybrids for Reversible NO_2 Sensing: Critical Role of pi-pi* Transition. *ACS Cent. Sci.* **2021**, *7*, 1176−1182.

(21) (a) Chen, A.; Liu, R.; Peng, X.; Chen, Q.; Wu, J. 2D Hybrid Nanomaterials for Selective Detection of NO_2 and SO_2 Using "Light On and Off" Strategy. *ACS Appl. Mater. Interfaces* **2017**, *9*, 37191−37200. (b) Fei, H.; Wu, G.; Cheng, W. Y.; Yan, W.; Xu, H.; Zhang, D.; Zhao, Y.; Lv, Y.; Chen, Y.; Zhang, L.; C, O. C.; Heng, C.; Chang, C. R.; Wu, H. C. Enhanced NO_2 Sensing at Room Temperature with Graphene via Monodisperse Polystyrene Bead Decoration. *ACS Omega* **2019**, *4*, 3812−3819.

(22) (a) Friedman, A. L.; Perkins, F. K.; Cobas, E.; Jernigan, G. G.; Campbell, P. M.; Hanbicki, A. T.; Jonker, B. T. Chemical vapor sensing of two-dimensional MoS_2 field effect transistor devices. *Solid State Electron.* **2014**, *101*, 2−7. (b) Wu, E.; Xie, Y.; Yuan, B.; Zhang, H.; Hu, X.; Liu, J.; Zhang, D. Ultrasensitive and Fully Reversible NO_2 Gas Sensing Based on p-Type $MoTe_2$ under Ultraviolet Illumination. *ACS Sens.* **2018**, *3*, 1719−1726.

(23) Tan, K.; Zuluaga, S.; Wang, H.; Canepa, P.; Soliman, K.; Cure, J.; Li, J.; Thonhauser, T.; Chabal, Y. J. Interaction of Acid Gases SO_2 and NO_2 with Coordinatively Unsaturated Metal Organic Frameworks: M-MOF-74 (M = Zn, Mg, Ni, Co). *Chem. Mater.* **2017**, *29*, 4227−4235.

(24) (a) Aylor, A. W.; Larsen, S. C.; Reimer, J. A.; Bell, A. T. An Infrared Study of NO Decomposition over Cu-ZSM-5. *J. Catal.* **1995**, *157*, 592−602. (b) Aylor, A. W.; Lobree, L. J.; Reimer, J. A.; Bell, A. T. In *An Infrared Study of NO reduction by CH_4 over Co-ZSM-5*, 11th International Congress On Catalysis - 40th Anniversary, Proceedings of the 11th ICC; Hightower, J. W.; Nicholas Delgass, W.; Iglesia, E.; Bell, A. T., Eds.; Studies in Surface Science and Catalysis, Elsevier, 1996; Vol. 101, pp 661−670. (c) Hadjiivanov, K.; Klissurski, D.; Ramis, G.; Busca, G. Fourier transform IR study of NOx adsorption on a CuZSM-5 DeNOx catalyst. *Appl. Catal., B* **1996**, *7*, 251−267. (d) Hadjiivanov, K. I. IR study of CO and NOx sorption on Ag-ZSM-5. *Microporous Mesoporous Mater.* **1998**, *24*, 41−49. (e) Hadjiivanov, K. I. Identification of Neutral and Charged N_xO_y Surface Species by IR Spectroscopy. *Catal. Rev.* **2000**, *42*, 71−144.

(25) (a) Nakamoto, K.; Griffiths, P. R. Infrared andRaman Spectra of Inorganic and Coordination Compounds. In *Handbook of Vibrational Spectroscopy* 2001. (b) Jensen, S.; Tan, K.; Feng, L.; Li, J.; Zhou, H. C.; Thonhauser, T. Porous Ti-MOF-74 Framework as a Strong-Binding Nitric Oxide Scavenger. *J. Am. Chem. Soc.* **2020**, *142*, 16562−16568.

(26) (a) Meng, Z.; Stolz, R. M.; Mirica, K. A. Two-Dimensional Chemiresistive Covalent Organic Framework with High Intrinsic Conductivity. *J. Am. Chem. Soc.* **2019**, *141*, 11929−11937. (b) Han, Y.; Chen, Y. L.; Ma, Y. J.; Bailey, J.; Wang, Z.; Lee, D. N.; Sheveleva, A. M.; Tuna, F.; McInnes, E. J. L.; Frogley, M. D.; Day, S. J.; Thompson, S. P.; Spencer, B.; Nikiel, M.; Manuel, P.; Crawshaw, D.; Schroder, M.; Yang, S. H. Control of the pore chemistry in metal-organic frameworks for efficient adsorption of benzene and separation of benzene/cyclohexane. *Chem* **2023**, *9*, 739−754. (c) Su, X.; Zhong, Z.; Yan, X.; Zhang, T.; Wang, C.; Wang, Y. X.; Xu, G.; Chen, L. Facile Synthesis of Metallosalphen-Based 2D Conductive Metal-Organic Frameworks for NO_2 Sensing: Metal Coordination Induced Planarization. *Angew. Chem., Int. Ed.* **2023**, *62*, No. e202302645.

(27) (a) Hsu, S. C. N.; Chang, Y. L.; Chuang, W. J.; Chen, H. Y.; Lin, I. J.; Chiang, M. Y.; Kao, C. L.; Chen, H. Y. Copper(I) nitro complex with an anionic [HB(3,5-Me_2Pz)$_3$] ligand: a synthetic model for the copper nitrite reductase active site. *Inorg. Chem.* **2012**, *51*, 9297−9308. (b) Timmons, A. J.; Symes, M. D. Converting between the oxides of nitrogen using metal-ligand coordination complexes. *Chem. Soc. Rev.* **2015**, *44*, 6708−6722. (c) Wright, A. M.; Sun, C.; Dinca, M. Thermal Cycling of a MOF-Based NO Disproportionation Catalyst. *J. Am. Chem. Soc.* **2021**, *143*, 681−686.

(28) (a) Xu, F.; Ho, H. P. Light-Activated Metal Oxide Gas Sensors: A Review. *Micromachines* **2017**, *8*, 333. (b) Kumar, R.; Liu, X.; Zhang, J.; Kumar, M. Room-Temperature Gas Sensors Under Photo-activation: From Metal Oxides to 2D Materials. *Nano-Micro Lett.* **2020**, *12*, No. 164.

(29) (a) Hansen, B. J.; Kouklin, N.; Lu, G. H.; Lin, I. K.; Chen, J. H.; Zhang, X. Transport, Analyte Detection, and Opto-Electronic Response of p-Type CuO Nanowires. *J. Phys. Chem. C* **2010**, *114*, 2440−2447. (b) Chen, Y.; Zhang, X.; Liu, Z.; Zeng, Z.; Zhao, H.; Wang, X.; Xu, J. Light enhanced room temperature resistive NO(2) sensor based on a gold-loaded organic-inorganic hybrid perovskite incorporating tin dioxide. *Mikrochim. Acta* **2019**, *186*, No. 47. (c) Ma, H. N.; Yu, L. M.; Yuan, X.; Li, Y.; Li, C.; Yin, M. L.; Fan, X. H. Room temperature photoelectric NO_2 gas sensor based on direct growth of walnut-like In_2O_3 nanostructures. *J. Alloys Compd.* **2019**, *782*, 1121−1126.

https://doi.org/10.1021/jacs.3c05095
J. Am. Chem. Soc. 2023, 145, 19293−19302